Electronic and Structural Origin of Ultraincompressibility of 5*d* Transition-Metal Diborides MB_2 (M = W, Re, Os)

Xing-Qiu Chen,[1] C. L. Fu,[1] M. Krčmar,[2] and G. S. Painter[1]

[1]*Materials Science and Technology Division, Oak Ridge National Laboratory, Oak Ridge, Tennessee 37831-6114, USA*
[2]*Department of Physics, Grand Valley State University, Allendale, Michigan 49401-9403, USA*

(Received 27 September 2007; published 16 May 2008)

First-principles theory was used to investigate the roles of bond topology and covalency in the phase stability and elastic strength of 5*d* transition-metal diborides, focusing on elements (M = W, Re, Os) that have among the lowest compressibilities of all metals. Among the phases studied, the ReB_2-type structure exhibits the largest incompressibility (c axis), comparable to that of diamond. This ReB_2 structure is predicted to be the ground-state phase for WB_2 and a pressure-induced phase (above 2.5 GPa) for OsB_2. Both strong covalency and a zigzag topology of interconnected bonds underlie these ultraincompressibilities. Interestingly, the Vickers hardness of WB_2 is estimated to be similar to that of superhard ReB_2.

DOI: 10.1103/PhysRevLett.100.196403 PACS numbers: 71.20.Be, 61.50.Lt, 62.20.D−, 71.15.Mb

The properties of ultra- and superhard materials clearly relate to strong covalent bonding in stabilizing particular structures. The classic example of the hardest known material, diamond (strong covalent bonds of tetrahedral sp^3 hybrid states), compared with graphite (strong, but planar sp^2 bonds) illustrates the important role of bond directionality. The next hardest materials known, c-BN and c-BC_2N, further exemplify the role of directional covalency among B, N, and C. In contrast to covalent bonds, metallic and ionic bonds are often associated with softer materials. For example, although the low compressibility 5*d* transition metals W, Re, and Os are characterized by the existence of directional metallic bonds, the mechanical strength of each is much lower (by a significant factor) than that of covalent materials. The alloying of B, C, and N with the so-called hard transition metals, however, is known to give strongly enhanced mechanical strength and hardness of each compound over that of the corresponding metal, as the crystal structure becomes more complex and directional hybridization of metal d electrons with anion s, p electrons occurs. In the following, we systematically explore the roles of covalency and structure in the stability and strength of the phases of a series of 5*d* transition-metal diborides with focus on the three transition metals (W, Re, and Os) with compressibilities among the lowest for metals.

Recently, two ultraincompressible, hard compounds OsB_2 and ReB_2 have been synthesized [1,2], both having high bulk moduli (360–395 GPa). Particular interest lies in ReB_2, which exhibits linear incompressibility along the c axis with a magnitude comparable to that of diamond [2], as well as a high hardness of 48 ± 5.6 GPa [2]. Interestingly, OsB_2 and ReB_2 form different lattice structures (cf. Fig. 1): OsB_2 with the orthorhombic RuB_2-type structure [1] (Orth: space group $Pmmn$), whereas ReB_2 crystallizes in the hexagonal ReB_2-type structure [2] (Hex-I: space group $P6_3/mmc$). The former has recently been investigated by first-principles calculations [3–7], that are consistent in relating the incompressibility of OsB_2 to strong covalent B-B and Os-B bonds. The electronic structure of OsB_2 and ReB_2 has also been determined [8].

In this work, we solve the local density equations to systematically investigate the structural, elastic, and electronic properties of the diborides (MB_2) of neighboring 5*d* transition metals (M = Hf, Ta, W, Re, Os, Ir). This study explains the origin of the ultraincompressibility in ReB_2 and identifies new diborides that also exhibit ultrahigh c-axis incompressibility. In these six diborides, the AlB_2-type hexagonal structure (Hex-II: space group $P6/mmm$) has previously been reported for Hf, Ta, and

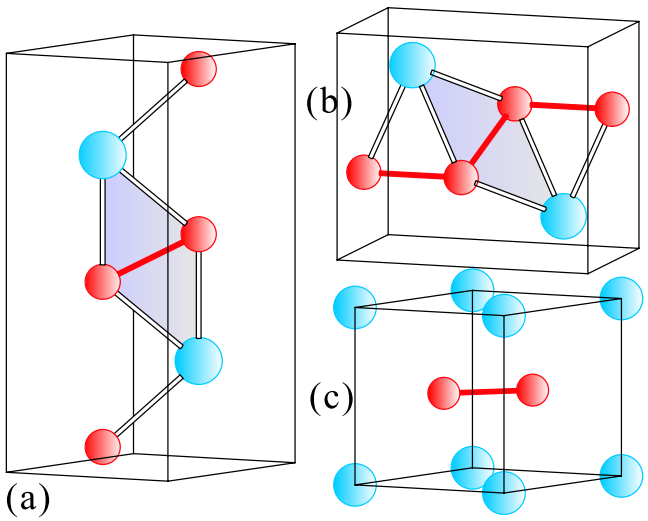

FIG. 1 (color online). Crystal structures of (a) ReB_2-type (Hex-I), (b) RuB_2-type (Orth), and (c) AlB_2-type (Hex-II). There is a similarity between Hex-I and Orth structures, as emphasized by the shaded area in (a) and (b). The larger (open) and smaller (filled) spheres indicate transition-metal and B atoms, respectively, in each outlined unit cell.

W diborides [9–11]. No experimental structural data is available for IrB_2 in the literature; thus, it is included in our study for comparison and reference as a possible stable phase. We note that, in terms of the local geometry, there is a similarity between the Hex-I and Orth structures, as emphasized by the shaded areas in Fig. 1. Among these three structures, we find the ReB_2-type structure (i.e., Hex-I) to exhibit the largest incompressibility along the c axis for W, Re, and Os diborides, comparable to that of diamond. We predict that WB_2 in this structure is also superhard with a hardness value similar to that of ReB_2. The origin of the c-axis ultraincompressibility correlates not only with the strong covalency of B-B and M-B bonds, but also with the local buckled structure of interconnected covalent bonds.

Our first-principles calculations were performed using the Vienna *ab initio* Simulation Package (VASP) [12] with the ion-electron interaction described by the projector augmented wave potential. We used both the generalized gradient approximation (GGA [13]) and local density approximation (LDA [14]) for the exchange-correlation functional.

Figure 2(a) presents the calculated heats-of-formation for three competing structures, Hex-I, Hex-II, and Orth, of MB_2 (M = Hf, Ta, W, Re, Os, and Ir) compounds. As shown in Fig. 2(a), the Hex-I and Orth structures are very close in energy for all MB_2 compounds studied here. Also, while the Hex-II structure is far more stable than the Orth and Hex-I phases for early 5d diborides (i.e., HfB_2 and TaB_2), the Hex-I structure is most energetically favorable phase for the midrow 5d diborides (i.e., WB_2 and ReB_2). With an increasing number of valence electrons (i.e., OsB_2 and IrB_2), the Orth structure becomes marginally more stable with respect to the Hex-I structure and the Hex-II structure becomes more unfavorable. The calculated structural stability trends are consistent with experiments for HfB_2 (Hex-II) [9], TaB_2 (Hex-II) [10], ReB_2 (Hex-I) [2], and OsB_2 (Orth) [1]. For WB_2, however, although the Hex-II structure has been reported as the experimental ground state [11], our calculations show that the Hex-II structure is actually the least stable phase compared with both Hex-I and Orth phases at zero pressure [Fig. 2(b)]. It has been reported that WB_2 can also be stabilized in the WB_2-type structure (space group: $P63/mmc$) [15] (consistent with first-principles results [7]). However, our calculations predict that the WB_2-type phase is energetically less stable by 1.1 kJ/mol-atom than the Hex-I (ReB_2-type) and Orth (RuB_2-type) phases. Calculation of the phonon spectrum shows no soft phonon induced instability, further confirming the structural stability of WB_2 in the Hex-I phase.

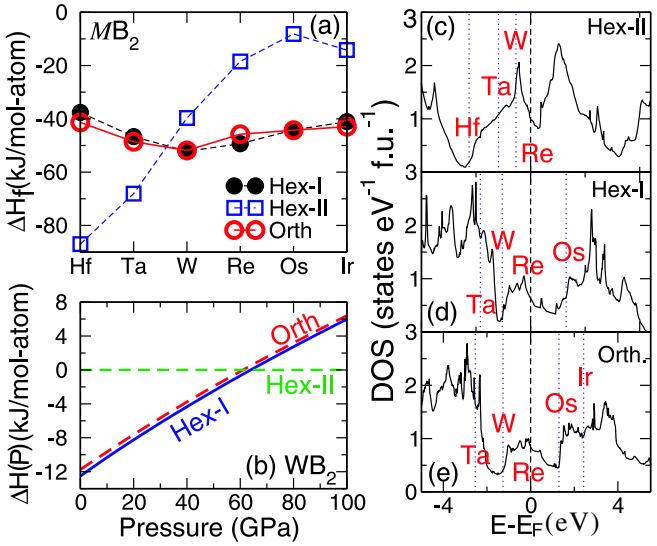

FIG. 2 (color online). Heats-of-formation (ΔH_f) at zero pressure of MB_2 (M = Hf, Ta, W, Re, Os, Ir) in ReB_2-type (Hex-I), AlB_2-type (Hex-II), and RuB_2-type (Orth) structures (a), enthalpies [$\Delta H(P)$] of different structures of WB_2 as a function of pressure relative to that of the Hex-II phase (b), and electronic density-of-states of MB_2 [from (c) to (e)] in Hex-II, Hex-I, and Orth structures, respectively. In (c)–(e), the energy zero is chosen as the Fermi energy (E_F) of ReB_2 and the corresponding Fermi levels of other MB_2 are represented by dashed lines.

The trends in the structural stability of MB_2 compounds can be understood from the electronic structure. The density-of-states (DOS) profiles of ReB_2 in the Hex-I, Hex-II, and Orth structures are shown in Figs. 2(c)–2(e), where the position of the Fermi level (E_F) is chosen as the reference energy zero. We note that the DOS profiles of the Hex-I and Orth structures are very similar: a wide valley separates the Re-B (as well as B-B) bonding and antibonding states. The states near E_F for ReB_2 in the Hex-I and Orth structures are the nonbonding Re d orbitals localized on the Re atoms in layers parallel to the basal plane. The DOS profile for the Hex-II structure, on the other hand, differs from those of the Hex-I and Orth structures by the presence of a deeper minimum about 3 eV below E_F. We find that the DOS of other MB_2 compounds can be well represented by the DOS profiles of ReB_2, but with a shift in the position of E_F as determined from the number of valence electrons (i.e., rigid band model; see Fig. 2). Since the E_F of WB_2, ReB_2, and OsB_2 fall in the DOS valley region for the Hex-I and Orth structures, the stabilization of the midrow 5d diborides is largely due to the fact that the B-B and M-B bonding states are fully occupied. Note that the wide separation between bonding and antibonding states in the DOS profiles of the Hex-I and Orth structures is a result of strong M-B and B-B interactions. The bonding characteristics and bond topology will be discussed later in conjunction with the magnitude and anisotropy of the calculated elastic constants. For the Hex-II structure, the E_F of HfB_2 is located at the middle of the gap separating the B-B bonding and antibonding states; thus, HfB_2 attains the lowest (most negative) heat of formation among all MB_2.

From the energy-versus-volume curves for the W and Os diborides, there are crossings between competing structures, signifying structural phase transformations under pressure. For WB_2, we predict a phase transition from Hex-I to Hex-II at $P = 65$ GPa, i.e., the experimentally reported Hex-II phase [11] of WB_2 is actually the high-pressure phase [Fig. 2(b)]. For OsB_2, although the Orth phase is the stable ambient phase at $P = 0$, the Orth phase is found to transform into the Hex-I phase at $P = 2.5$ GPa.

In Fig. 3 the calculated elastic constants are summarized for MB_2 compounds in the Hex-I structure (WB_2, ReB_2, and OsB_2), Orth structure (WB_2, ReB_2, OsB_2, and IrB_2), and Hex-II structure (all MB_2 compounds except for IrB_2). The plot shows that each of the global ground-state structures of the six 5*d* diborides is elastically stable at zero pressure. For the elastic constants of Orth OsB_2, there is good agreement with results from previous work [3–6].

For W, Re, and Os diborides in the Hex-I structure, we find unusually high incompressibilities along the *c* axis, as demonstrated by the extremely large C_{33} values (cf. Fig. 3). Among the 5*d* diborides, the Hex-I phase ReB_2 has the highest C_{33} value of 1094 GPa, comparable with that of diamond ($C_{33} = 1079$ GPa [16]). Measurements reported for ReB_2 (*c* axis) also approach that of diamond [2]. Here, we further demonstrate that WB_2 and OsB_2 in the Hex-I structure also have extremely high C_{33} values, differing from that of the Hex-I ReB_2 by less than 10%. As mentioned, this Hex-I structure is the ground-state phase for WB_2 and a pressured-induced phase for OsB_2. Also, it is interesting to note that, for W, Re, and Os diborides, the C_{33} values of the Orth structure are only slightly lower (by about 100 GPa) than those of the Hex-I structure, suggesting that a common feature in the electronic structure contributes to their high C_{33} values. By comparison, the elastic constants (C_{11} and C_{22}) for deformation along the *a* and *b* axis in the Hex-I and Orth structures of the midrow 5*d* diborides are about 300–400 GPa lower than their C_{33} counterparts.

For the Hex-II phase, all the diborides considered here have similar C_{33} values ranging from 450 to 500 GPa, which is just half that of the Hex-I structure of W, Re, and Os diborides (Fig. 3). The C_{11} and $C_{11} + C_{12}$ values of the Hex-II structure, on the other hand, are very close to (and, in most cases, slightly larger than) their counterparts of the Hex-I and Orth structures of W, Re, Os diborides (Fig. 3).

For discussion of the bonding mechanism in 5*d* diborides, we use ReB_2 as an illustrative case. In order to clearly identify the chemical bond character, we calculate the electronic localization function (ELF) [17], which is based on a topological analysis related to the Pauli exclusion principle. An ELF = 1 corresponds to perfect electron localization. The contours of ELF domains for the Orth, Hex-I, and Hex-II structures on their respective close-packed planes are shown in Fig. 4. We note strong B-B covalent bonds in all structures, with nearly identical B-B covalent "point attractors" at ELF = 0.85. However, fundamental differences separate the Hex-I (or Orth) and Hex-II structures: (1) the B atoms form nonplanar graphitelike layers perpendicular to the *c* axis in both the Hex-I and Orth structures, whereas the B-B covalent bonds in the Hex-II structure form perfect hexagonal planar layers parallel to the basal plane; and (2) the B atoms have four Re atoms each as nearest neighbors (with short bond distances about 2.2 Å) in the Hex-I and Orth structures, but have six nearest neighbor Re atoms in the Hex-II structure. Our analysis shows that stronger Re-B bonds

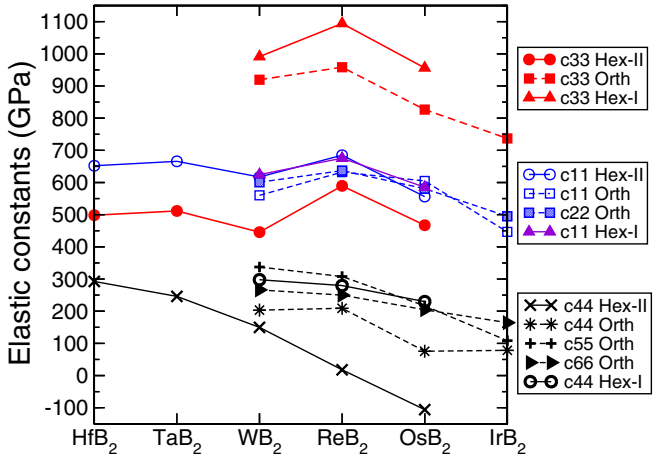

FIG. 3 (color online). Calculated LDA elastic constants of the ReB_2-type (Hex-I), RuB_2-type (Orth), and AlB_2-type (Hex-II) structures for the MB_2 compounds (M = Hf, Ta, W, Re, Os, Ir). Not shown in the plot are the C_{12} and C_{13} of these three structures and the C_{23} of the Orth structure; these elastic constants have values in the range of 200–300 GPa for W, Re, and Os diborides.

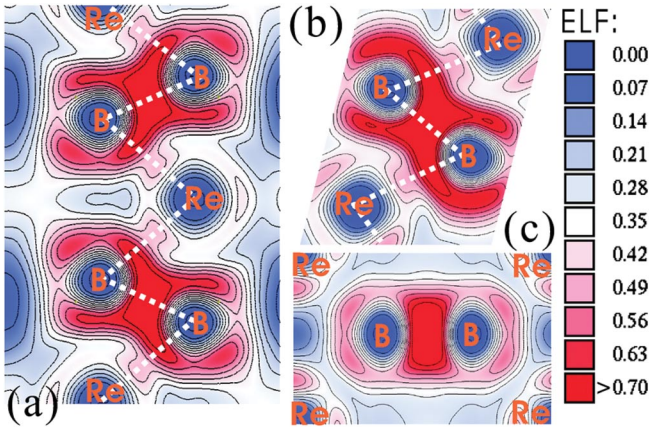

FIG. 4 (color). Contours of electron localization function (ELF) of ReB_2 on: (a) the (110) plane of the ReB_2-type (Hex-I) structure, (b) the plane corresponding to the shaded area of Fig. 1(b) of the RuB_2-type (Orth) structure, and (c) the (110) plane of the AlB_2-type (Hex-II) structure. The zigzag chains in (a) and (b) are drawn to emphasize the alternating directionality of the network of strong interconnected B-B, Re-B bonds.

relate to B-coordination with a smaller number of Re nearest neighbors. This becomes evident in comparing the contour plot of ELF domains between Hex-I [Fig. 4(a)] and Hex-II [Fig. 4(c)] structures. In the Hex-I structure, there exist well-defined zigzag covalent chains [emphasized by the white dashed lines in Fig. 4(a)] along the c direction, interconnected by shared B and Re atoms. There are also Re-B covalent bonds directly along the c axis [Fig. 4(a)], although not as strong as the Re-B bonds in the chains. Furthermore, since B atoms in the Hex-I structure are not inversion symmetry sites, the hexagonal B layers necessarily become nonplanar with B atoms strongly buckled towards the Re atoms that are interconnected by Re-B bonds in the chains. In other words, the B-B bonding is strongly complemented by the Re-B covalent bonds in the Hex-I structure. Similarly, for the Orth structure, the contours of the ELF domains [cf. Fig. 4(b)] on the shaded area of Fig. 1(b) show nearly identical features as those in the Hex-I structure: local buckled B layer structures interconnected with zigzag B-Re and B-B covalent bonds.

In contrast, for the Hex-II structure, the B atoms are at sites with inversion symmetry, and the B atom has a higher coordination number of Re atoms than in the Hex-I and Orth structures. The ELF analysis shown in Fig. 4 indicates that the Re-B bonds are considerable weaker in the Hex-II structure than those in the zigzag chains of the Hex-I and Orth structures (thus a much lower C_{33} value for the Hex-II structure).

The bulk and shear moduli are often used as indicators of material hardness. It has been suggested [18] that a linear correlation exists between the shear modulus and the Vickers hardness for many of the known high-strength materials. Assuming this linear correlation, and using the calculated LDA (GGA) shear modulus of 295 (281) GPa of ReB_2, we estimate that ReB_2 has a Vickers hardness of 47.5 (45.2) GPa, which is in surprisingly good agreement with the experimental value [2] (48 ± 5.6 GPa). This agreement, however, may be coincidental, since the strains associated with the hardness measurement are beyond the elastic limit. Nevertheless, the shear moduli are routinely used for the purpose of a comparative measure of the stress needed for plastic flow, in particular, among materials with the same lattice structure. The LDA (GGA) shear moduli of WB_2 and OsB_2 in the ReB_2-type structure were calculated to be 294 (273) and 216 (205) GPa, respectively. Similarly, using the calculated shear moduli, we obtained the Vickers hardness of 47.4 (43.8) GPa for WB_2 and 33.7 (31.8) GPa for OsB_2. Therefore, we predict that WB_2 is also a superhard material with a hardness value similar to that of ReB_2. Our estimated hardness of WB_2 is considerably higher than that measured by Okada *et al.* [19]. However, we notice that their measured hardness (21.3 GPa) of the so-called WB_2 samples [19] is for W borides with a defective W_2B_5-type structure (i.e., not for the ideal ReB_2-type structure) and contain less boron than indicated by the formula. Therefore, their measured results cannot be compared directly with our estimated value.

Research sponsored by the Division of Materials Sciences and Engineering, U.S. Department of Energy under contract with UT-Battelle, LLC.

[1] R. W. Cumberland *et al.*, J. Am. Chem. Soc. **127**, 7264 (2005).
[2] H.-Y. Chung *et al.*, Science **316**, 436 (2007).
[3] Y. Z. Chen *et al.*, Phys. Rev. B **74**, 012102 (2006).
[4] M. Hebbache, L. Stuparevic, and D. Zivicovic, Solid State Commun. **139**, 227 (2006).
[5] S. Chiodo *et al.*, Chem. Phys. Lett. **425**, 311 (2006).
[6] H. Guo *et al.*, Appl. Phys. Lett. **88**, 221904 (2006).
[7] X. Hao *et al.*, Phys. Rev. B **74**, 224112 (2006).
[8] A. L. Ivanovskii and N. I. Medvedeva, Russ. J. Inorg. Chem. **44**, 1633 (1999).
[9] L. Bsenko and T. Lundstroem, J. Less-Common Met. **34**, 273 (1974).
[10] B. Loennberg and T. Lundstroem, J. Less-Common Met. **139**, L7 (1988).
[11] H. P. Woods, F. E. Wawner, Jr., and B. G. Fox, Science **151**, 75 (1966).
[12] G. Kresse and D. Joubert, Phys. Rev. B **59**, 1758 (1999), and references therein.
[13] J. P. Perdew *et al.*, Phys. Rev. B **46**, 6671 (1992).
[14] D. M. Ceperley and B. J. Alder, Phys. Rev. Lett. **45**, 566 (1980).
[15] T. Lundstroem, Arkiv. Kemi **30**, 115 (1969).
[16] H. T. McSkimin and P. Andreatch, J. Appl. Phys. **43**, 985 (1972).
[17] B. Silvi and A. Savin, Nature (London) **371**, 683 (1994).
[18] D. M. Teter, MRS Bull. **23**, 22 (1998).
[19] S. Okada, K. Kudou, and T. Lundström, Jpn. J. Appl. Phys. **34**, 226 (1995).